Title

Synthetic mycobacterial molecular patterns work synergistically to recapitulate complete Freund's adjuvant

Authors/Affiliations

Jean-Yves Dubé [1,2,3*], Fiona McIntosh [2,3], Juan G. Zarruk [4], Samuel David [4], Jérôme Nigou [5], Marcel A. Behr [1,2,3,6*]

1, Department of Microbiology and Immunology, McGill University. 2, Infectious diseases and Immunity in Global Health Program, Research Institute of the McGill University Health Centre. 3, McGill International TB Centre. 4, Centre for Research in Neuroscience, Research Institute of the McGill University Health Centre. 5, Institut de Pharmacologie et de Biologie Structurale, Université de Toulouse, CNRS, Université Paul Sabatier, Toulouse, France. 6, Department of Medicine, McGill University Health Centre, Montréal, Canada.

Contact Info*

jean-yves.dube@mail.mcgill.ca
marcel.behr@mcgill.ca
McGill University Health Centre
1001 boul. Décarie
Glen Site Block E, Office #EM3.3212
Montréal, Québec, Canada
H4A 3J1

Abstract

Complete Freund's adjuvant (CFA) has historically been one of the most useful tools of immunologists. Essentially comprised of dead mycobacteria and mineral oil, we asked ourselves what is special about the mycobacterial part of this adjuvant, and could it be recapitulated synthetically? Here, we demonstrate the essentiality of *N*-glycolylated peptidoglycan plus trehalose dimycolate (both unique in mycobacteria) for the complete adjuvant effect using knockouts and chemical complementation. A combination of synthetic *N*-glycolyl muramyl dipeptide and minimal trehalose dimycolate motif GlcC14C18 was able to induce experimental autoimmunity qualitatively similar to the whole mycobacteria in CFA. This research outlines how to replace CFA with a consistent, molecularly defined adjuvant which may inform the design of immunotherapeutic agents and vaccines benefitting from cell-mediated immunity. We also anticipate using synthetic microbe-associated molecular patterns (MAMPs) to study mycobacterial immunity and immunopathogenesis.

Introduction

Infection with *Mycobacterium tuberculosis*, or administration of bacille Calmette-Guérin (BCG), normally leads to cell-meditated immunity (CMI) to the corresponding bacterial antigens. The tuberculin skin test is positive when the immune response, a type IV hypersensitivity reaction or delayed-type hypersensitivity (DTH), occurs to tuberculin (a protein extract of *M. tuberculosis*). This "cutaneous sensitivity" was closely examined in the 1940s using complete Freund's adjuvant (CFA, heat-killed *M. tuberculosis* in mineral oil plus surfactant) [1, 2]. These studies provided the first direct evidence for the cellular nature of DTH by transfer from a CFA-immunized guinea pig to a naïve one only through the washed, heat-liable cellular fraction of peritoneal exudates [1, 2]. It is now known that DTH is mediated specifically by antigen-sensitive T cells.

Today, CFA is a 'gold standard' adjuvant for eliciting CMI in research models of autoimmune disease. Notable is the experimental autoimmune encephalomyelitis (EAE) model of T-cell meditated destruction of myelin causing ascending paralysis, used most often to model multiple sclerosis [3, 4]. CFA is not used in humans because of high reactogenicity [5]. We have asked ourselves: what was the impetus for Jules Freund to develop his eponymous adjuvant with *M. tuberculosis*? For those conducting TB research, it is well appreciated that handling *M. tuberculosis* (a slow growing, clumping, fastidious, and lethally pathogenic organism) is a significant task *per se*. So, why did Freund choose to incorporate these bacteria?

Effort has been made to describe the microbe-associated molecular patterns (MAMPs) in mycobacteria that drive the adjuvant effect. Evidence has pointed to mycobacterial peptidoglycan (PGN), specifically down to the molecular motif muramyl dipeptide (MDP) [6, 7]. Mycobacteria are distinct in that they produce the *N*-glycolyl MDP motif in their cell wall [8, 9, 10] and this PGN modification has been shown to be more potent compared to the common *N*-acetyl MDP motif possessed by other bacteria [7, 11]. MDP is thought to be recognized through the host molecule NOD2 [12], and mutations in NOD2 predispose humans to increased risk of mycobacterial and inflammatory diseases [13, 14, 15, 16]. Alternatively, others have pointed to the mycobacterial cell wall lipid trehalose-6,6-dimycolate (TDM) alone or synergistically with purified peptidoglycan [17]. TDM is recognized by the host with the C-type lectin Mincle in concert with FcRγ and MCL [18, 19]. TDM has been demonstrated in animal models to alone be sufficient for granuloma formation and immunopathological responses [18, 20].

Both *N*-glycolyl MDP and TDM are MAMPs unique to mycobacteria. Their role in mycobacterial immune responses is supported by the literature and their host receptors are well-known. Additionally, *N*-glycolyl MDP is producible synthetically [7, 21, 22]. Recently a minimal motif of TDM called GlcC14C18 was produced synthetically and shown to retain adjuvancy but with minimal toxicity [23]. As a complex biologic, CFA is subjected to batch inconsistency. We hypothesized that it is possible to create an entirely synthetic CFA using a rational approach to identify essential MAMPs to replace the whole mycobacteria in the adjuvant. In this work, we establish the necessity for *N*-glycolylation of PGN, NOD2 and Mincle for full CFA adjuvancy. We also demonstrate that the mycobacteria in CFA can be replaced with synthetic *N*-glycolyl MDP and GlcC14C18 to at least partially restore the adjuvant effect in both a murine model of antigen-specific T-cell immunity as well as the EAE model of autoimmune ascending paralysis.

MAMPs worked synergistically, highlighting the need for considering more than one MAMP in adjuvant design. An entirely synthetic adjuvant may benefit animal experiments currently using CFA as well as indicate how to translate the CFA effect into products for human use. We suggest such synthetics may be used to dissect immuno-pathogenesis of mycobacterial diseases.

Results

N-glycolylation of PGN is required for complete mycobacterial adjuvancy

Previous work from our group indicated mycobacteria required *N*-glycolylated PGN to elicit a maximal immune response during live infection [7, 11]. To determine if CMI elicited from dead mycobacteria in the context of Freund's adjuvant similarly required *N*-glycolylated PGN, we prepared in-house complete Freund's adjuvant with heat-killed *M. tuberculosis* strain H37Rv, and H37Rv Δ*namH*. NamH is the enzyme responsible for *N*-glycolylation of PGN units as they are being synthesized in the cytoplasm, and the Δ*namH* mutant has been characterized previously to be devoid of *N*-glycolylation [11] (fig. 1A). We immunized mice against ovalbumin (OVA, an exemplary antigen) with our CFAs, and also with incomplete Freund's adjuvant (IFA, lacks mycobacteria), and examined the OVA-specific T-cell response in the draining lymph nodes seven days later through hallmark cytokine production (fig. 1B; gating in fig. S1). We focused on CD4+CD8- cells because they could significantly produce different cytokines (IL-4, IL-10 and IL-17A in addition to IFN-γ). CD4+CD8- cells were generally the majority OVA-specific IFN-γ producing lymph node cell population and showed greater difference between CFA and IFA immunized mice in terms of OVA-specific IFN-γ (not shown). CD4+CD8- cell responses also correlated very well with IFN-γ ELISpot when tested (not shown). Maximum OVA-specific IFN-γ production from CD4+ T cells was depended on mycobacteria and *namH*; OVA-specific IL-17A was strongly dependent on mycobacteria, but did not depend on *namH* (fig. 1C). We show both percentages and numbers of cells because incorporation of mycobacteria into IFA induced increased lymphocyte numbers in the draining lymph nodes (fig. S2). The data show that *namH* contributes to about one third of mycobacterial-dependent antigen-specific IFN-γ in CD4+ cells (fig. S3). OVA-specific IL-4 and IL-10 were weakly dependent on mycobacteria, but not clearly on *namH* (fig. S2). This is consistent with the hypothesized role for mycobacteria being a key ingredient in CFA for eliciting CMI, and that mycobacterial PGN modification by NamH makes a more potent adjuvant.

Host *Nod2* is required for complete mycobacterial adjuvancy

Recognition of mycobacteria during live infection requires the host molecule NOD2 [24]. Because we hypothesize mycobacterial PGN plays a role in CFA adjuvancy, specifically the MDP motif where *N*-glycolylation occurs, we addressed whether the PGN/MDP sensor NOD2 is important for CFA adjuvancy in our OVA model. *Nod2*+/+ and *Nod2*-/- mice were immunized against OVA in the context of CFA or IFA of commercial provenance. OVA-specific IFN-γ from CD4+ cells of CFA-immunized mice required *Nod2* for maximal effect (fig. 2), and an independently produced IFN-γ ELISpot of total lymph node cells indicated that *Nod2* is required for about half of the adjuvancy contribution of mycobacteria in CFA (fig. S4A). In the absence of *Nod2*, OVA-specific IL-17A was also impaired in CFA-immunized mice (fig. 2). With IFA as adjuvant, IFN-γ and IL-17A responses were *Nod2*-independent as expected (fig. 2 and S4A).

No obvious phenotype was observed for IL-4 and IL-10 (fig. S4C). Together, these results corroborate the role for NOD2 and accordingly mycobacterial PGN in the ability of CFA to elicit CMI.

Host *Mincle* is required for complete mycobacterial adjuvancy

In the absence of *Nod2*, the adjuvant effect of mycobacteria declined partially, but not completely. Therefore, there is other mycobacterial MAMP recognition besides that through NOD2 which is important for the remainder CFA adjuvancy. Others have indicated that Mincle-mediated recognition of TDM contributes to mycobacterial adjuvancy [17]. We tested the dependence of our OVA-immunization model with *Mincle*-KO mice [25]. *Mincle*+/+ and *Mincle*-/- mice were immunized against OVA in the presence of CFA and IFA. CFA-elicited OVA-specific IFN-γ and IL-17A from CD4+ T cells was partially dependent on *Mincle* (fig. 3). Similar trends of smaller differences were also observed for IL-4 and IL-10 (fig. S5B). IFA-immunized mice showed *Mincle*-independent responses, as expected (fig. 3 and S5). These results implicate Mincle and thus its main mycobacterial ligand, TDM, in CFA adjuvancy as well. Therefore, at least two mycobacterial MAMPs, *N*-glycolylated PGN as well as TDM, are essential for the full adjuvant effect of mycobacteria in the context of CFA.

Synthetic mycobacterial NOD2 and Mincle ligands can complement IFA to increase antigen-specific T-cell responses.

We have demonstrated that NOD2 and Mincle signalling are essential for the full adjuvant effect of CFA. From this line of thought, we hypothesized that IFA can be complemented with pure NOD2 and/or Mincle ligands to recapitulate some or all of the adjuvant effect of whole mycobacteria. We initially attempted to complement IFA with *N*-glycolyl MDP alone and TDM alone in our OVA model; neither of these MAMPs produced substantial OVA-specific responses over the IFA baseline in the draining lymph nodes on their own (not shown). TDM administration was limited by pathological inflammation at the injection site with increasing doses, occurring at 10 µg and higher, which is not observed with CFA injection (fig. S6). Recently, a rationally determined minimal chemical structure of TDM for Mincle recognition was produced (called GlcC14C18) (fig. 4A and B) which was reported to retain activity as a Mincle agonist without the 'toxicity' associated with TDM [23]. We compared TDM and GlcC14C18 at a 10 µg dose in *Mincle*+/+ and *Mincle*-/- mice to confirm if GlcC14C18 produced less pathological inflammation and whether inflammation was *Mincle*-dependent in our mouse model. Pathological inflammation at the injection site was only observed with TDM, was *Mincle*-dependent (fig. 4C), and worsened over the course of the experiment (fig. S7).

By examining cytokine production from dendritic cells *in vitro*, it became apparent to us that MDP and TDM elicit maximal immune responses when combined synergistically (fig. S8). Interestingly, GlcC14C18 also synergized with *N*-glycolyl MDP *in vitro* (fig. S8). Using minimal synthetic MAMPs for PGN (i.e. *N*-glycolyl MDP) and TDM (i.e. GlcC14C18), we complemented IFA to test if CMI could be achieved with a completely synthetic adjuvant containing these essential mycobacterial MAMPs. OVA-specific cytokine responses in CD4+ cells were higher with increasing doses of GlcC14C18 over a 30 µg *N*-glycolyl MDP dose, relative to MDP alone by flow cytometry (fig. 5); IFN-γ and IL-17A reached only near half of

the CFA level at the tested doses, but IL-4 and IL-10 were complemented sufficiently at 10 µg GlcC14C18. GlcC14C18 clearly induced lymphoproliferation in the draining lymph nodes (fig. S9A), and IFN-γ ELISpot corroborated results obtained with flow cytometry IFN-γ (fig. S9B). To be sure GlcC14C18 adjuvancy was enhanced by addition of MDP *in vivo*, we performed a titration of lower MDP doses on 10 µg GlcC14C18 which confirmed synergy between the synthetic mycobacterial MAMPs (fig. S10). These results show that mycobacterial adjuvancy in the context of CFA can be at least partially phenocopied synthetically with just two mycobacterial MAMPs: namely *N*-glycolyl MDP and GlcC14C18.

Synthetic mycobacterial MAMPs can induce EAE similar to CFA

We were able to partially complement IFA with synthetic mycobacterial MAMPs in our model of OVA immunization according to immunological readouts. One of the common uses of CFA is in animal models of autoantigen-specific autoimmunity. To determine if our synthetic formulation can phenocopy the effect of whole mycobacteria to produce a more complex biological outcome such as autoimmunity, and thereby provide further validation of the 'completeness' of the synthetic formula, we tested IFA + GlcC14C18 + *N*-glycolyl MDP against CFA in ability to induce relapsing-remitting EAE (RR-EAE). Briefly, mice were randomly immunized against myelin oligodendrocyte glycoprotein (MOG) synthetic peptide with CFA or IFA + 10 µg GlcC14C18 + 30 µg *N*-glycolyl MDP, and onset of RR-EAE was determined by clinically scoring ascending paralysis daily in a blinded manner (fig. 6A). Both CFA and IFA + GlcC14C18 + MDP produced RR-EAE that was indistinguishable except quantitatively: over the course of the experiment, the average EAE score was lower with the synthetic adjuvant compared to the CFA control (fig. 6B), with a cumulative score suggesting about half the disease burden (58% of CFA cumulative score) (fig. 6C). Expectedly, lower EAE scores also corresponded with less weight-loss (fig. S11A). Of note, there were mice in the synthetic adjuvant group that reached the same scores as in the CFA group, but fewer (fig. S11B). Therefore, GlcC14C18 and *N*-glycolyl MDP were sufficient to recapitulate the adjuvant effect of the whole mycobacterial cell in EAE, albeit quantitatively less at the tested doses of MAMPs. Additionally, we had attempted RR-EAE with IFA + TDM + MDP previously, which produced a far less compelling phenocopy of CFA (fig. S12). In our hands, the IFA + GlcC14C18 + *N*-glycolyl MDP adjuvant has both the advantage of being completely synthetic and more efficacious, than the TDM-containing adjuvant.

To verify if there were any overt qualitative histopathological differences in EAE between CFA and the synthetic adjuvant, we examined spinal cords from three mice from each adjuvant group, having EAE scores 2, 3 and 3.5 at harvest (disease profile of these mice in fig. S11C). Both cellular infiltrates and demyelination of the white matter looked equivalent between adjuvants upon visual inspection (fig. 7A). Mice with different EAE scores had correspondingly different areas of diseased tissue of the spinal cord (fig. 7B), but in comparing adjuvants there was no detectable difference in the area of diseased spinal cord tissue (with statistical power to detect as low as +/- 15% CFA levels) (fig. 7C). The main determining variable was EAE score, not adjuvant. Overall, we were not able to detect any overt differences in the autoimmune pathology created by IFA + GlcC14C18 + MDP compared to the gold standard CFA. Extrapolating histopathological data to all 30 the mice in our experiment, we would expect however that the synthetic adjuvant produced less pathology in the spinal cord on

231 average since EAE scores were lower on average. Whether this quantitative difference between
232 CFA and the synthetic formulation can be reduced with rigorous dose optimization is unclear.
233
234 **Discussion**
235
236 The ability of an adjuvant to elicit CMI can depend on ligand-receptor interactions,
237 specifically MAMP-PRR interactions. It is well appreciated since the hypothesis of Charles
238 Janeway Jr. that the host decision to mount an adaptive immune response requires genetically
239 inborn sensors to detect the presence of microbial products, or microbes by association, and that
240 this is the foundation of classical adjuvants including CFA [26]. These interactions can be thought
241 of as an "arms race" between host and microbe, originating through antagonistic evolution in the
242 case of immune evasion [27]. Additionally, we can imagine the case where a microbe might evolve
243 to increase a specific PRR interaction that favours a specific active immunological environment
244 necessary for its lifecycle. When mycobacteria interact with their host, either in the form of *M.*
245 *tuberculosis* infection, BCG vaccination or immunization using CFA, CMI normally occurs.
246 The immune response to mycobacteria has been attributed to its unique cell wall, especially the
247 MDP motif of PGN [6, 7, 11, 24] and TDM [17, 19]. We have shown in the context of CFA-induced
248 immunization and autoimmunity that synthetically produced *N*-glycolyl MDP and TDM
249 (GlcC14C18) can contribute synergistically to recapitulate the mycobacterial adjuvant effect.
250
251 There are also other mycobacterial MAMPs previously identified (and likely more yet
252 unidentified), plus a greater number of PRRs linked to these microbial products. The extent to
253 which some these MAMPs contribute to mycobacterial adjuvancy may be the subject of our
254 future studies. However, most are not yet producible synthetically. Purified ManLAM was
255 recently shown to elicit EAE in mice, dependent on the host C-type lectin Dectin-2 (Clec4n), at a
256 dose of 500 µg per animal [28]. Of note, we were not able yet to produce synthetic mimics of
257 ManLAM that induce Dectin-2 signaling [29]. Similarly, purified TDM has been used to elicit
258 EAE at 500 µg per mouse, mostly dependent on MCL (Clec4d) and partially on Mincle (Clec4e)
259 [19]. These findings support a role for mycobacterial MAMPs driving the CFA effect, but with the
260 requirement of purifying biologically-sourced MAMPs and such high doses, we are concerned
261 that these phenotypes might be partly driven by the inclusion of other contaminating MAMPs,
262 which we have shown can have activity between 1-10 µg *in vivo* when used synergistically (i.e.
263 even 1% impurity could alter results). TLR-2 has been documented to interact with multiple
264 mycobacterial lipids [30]. TLR-2 knockout mice have been used in EAE, but the literature is
265 inconsistent on whether TLR-2 promotes CFA-induced EAE [31, 32, 33, 34]. Mycobacterial DNA was
266 recently shown to signal through the cGAS/STING pathway after phagosomal disruption via
267 ESX-1 [35, 36]. In the context of Freund's adjuvant, it is not clear if heat-killed mycobacteria could
268 have cytosolic access to activate cGAS/STING. The IFA fraction perhaps could deliver MAMPs
269 across membranes. TLR-9 also senses DNA, and appears to play a role during *M. tuberculosis*
270 infection in mice [37], and in humans [38]. TLR-9 was also shown to be necessary for full induction
271 of EAE [31, 33]. As synthetic DNA is available, pursuing the role of DNA in mycobacterial
272 adjuvancy interests us, perhaps as a third synthetic MAMP to work with MDP and GlcC14C18.
273
274 Mycobacteria are not completely unique in possessing MAMPs that elicit CMI. As an
275 example, the tuberculosis vaccine candidate M72/AS01E utilizes monophosphoryl lipid A
276 (MPLA), a TLR-4 agonist based on lipopolysaccharide (LPS), to elicit CMI. LPS is made in

Gram negative bacteria, not mycobacteria. We concede that many microbes likely contain MAMPs able to elicit CMI; here we have concerned ourselves primarily with the history of mycobacterial adjuvancy and Jules Freund. It is conceivable that a combination of MAMPs from different bacteria could elicit 'unnatural' immunity that may be beneficial to control certain infectious agents that otherwise evade natural immune responses.

We were able to show that *N*-glycolylation of *M. tuberculosis* PGN altered the adjuvancy of the mycobacterial cell in the context of CFA. This is consistent with our previous work on the increased potency of mycobacterial PGN in other contexts [7, 11]. Interestingly, the benefit of *N*-glycolylation of PGN seemed primarily skewed toward IFN-γ production, and other Th cytokines showed limited change. This may indicate that mycobacteria retain *N*-glycolylation of PGN specifically to shift immune responses in a Th1 bias and should be further investigated during live infection. Corroboratively, *Nod2* was also necessary for full CFA adjuvancy, for IFN-γ but also cytokines indicative of other Th cell functionality. Together, this supports a role of mycobacterial PGN uniquely contributing to CFA adjuvancy. We were somewhat surprised that MDP emulsified by itself in IFA was insufficient to recapitulate the adjuvant effect of CFA. In a 1975 paper, *N*-acetyl MDP appeared sufficient in a guinea pig model to elicit DTH using OVA as antigen [6]. In 2009 using a very similar model, *N*-glycolyl MDP alone was sufficient to increase ELISpot IFN-γ to near CFA levels, while *N*-acetyl MDP failed [7]. One hypothesized explanation is the presence of contaminating MAMPs in certain preparations of OVA. To limit this potential issue, in the current investigations we have used Endotoxin-free/ultra-pure OVA. OVA is known to often come with a dose of endotoxin which affects the immunological outcome of experiments [39]. MDP alone was clearly not sufficient for us in our recent studies, and this is consistent with a large literature of *in vitro* experiments that show MDP works synergistically in most cellular responses.

Other groups have supported a role for TDM in mycobacterial adjuvancy [17, 19]. TDM together with purified PGN was shown to synergistically promote IL-17 production from OVA-specific (OT-II) CD4+ T cells adoptively transferred into congenic mice [17]. This and other work directed us to test Mincle-dependence of CFA and MDP synergy with TDM. *Mincle*-/- mice allowed us to infer that CFA adjuvancy required TDM for maximal effect for different Th-indicative cytokines including IFN-γ and IL-17A. TDM is thought to be the main Mincle ligand in mycobacteria, however, there are other ligands. Purified from H37Rv, trehalose-6,6'-monomycolate, glucose monomycolate, diacyl-trehalose and triacyl-trehalose were shown to stimulate mouse and human Mincle (plus glycerol monomycolate stimulates human Mincle only) [23]. It is possible that the phenotype of reduced immunity is because sensing of these other MAMPs is decreased. Nevertheless, we have shown Mincle signalling is essential for full CFA adjuvancy.

While *in vitro* assays showed clear synergy between TDM and MDP, *in vivo* experiments were limited by overt immunopathology from TDM. That TDM was able to synergize with MDP drove us to test GlcC14C18, which had been branded as a similarly efficacious, but non-toxic Mincle agonist [23]. GlcC14C18 together with *N*-glycolyl MDP was able to partly recapitulate CFA in the OVA model. Note also that the individual MAMPs had limited effect, and only together substantially showed complementation of IFA. This 'synergy' has excited us, and we are interested in further understanding the implications for MAMP signalling (which

MAMPs synergize together; what redundancy exists; do different synergies alter the Th type of CMI? Etc.). It is unclear why MDP plus GlcC14C18 completely complemented IL-4 and IL-10, while CFA immunized *Nod2*-/- and *Mincle*-/- mice showed only small, generally insignificant defects for IL-4 and IL-10 compared to wild-type. Natural TDM might lack promotion of IL-4/IL-10 axes of Th immunity, consistent with the observed 'toxicity'. IFN-γ and IL-17A were not fully complemented with the tested doses of MDP and GlcC14C18. An optimal, or mycobacterial-representative, dose of these MAMPs may not have been reached. With the complexity of two MAMPs and the biological variability in our model, we did not find clearly better doses than those tested in EAE. Other mycobacterial MAMPs may be necessary to fully recapitulate the adjuvant effect of whole mycobacteria, which have been mentioned above.

With the wholly synthetic formulation of 10 µg GlcC14C18 plus 30 µg *N*-glycolyl MDP, we were able to induce RR-EAE in mice that was qualitatively indistinguishable from that induced with CFA (in terms of ascending paralysis induced, and spinal cord pathology), but milder overall (lower average EAE scores or disease burden). That the synthetically induced EAE was less severe correlated with incomplete complementation in the OVA model using the synthetic adjuvant. EAE that was attempted with TDM plus MDP earlier (which worked poorly) was also less potent in the OVA model than the synthetic formulation, further indicating correlation between these readouts (not shown). CFA often needs to be 'titrated' to account for batch-dependent efficacy in our experience, and EAE of the level seen with the synthetic adjuvant occurs sometimes with weaker CFA batches (not shown). CFA with higher concentrations of mycobacteria (i.e. 4 mg/ml) is also used when a more severe, chronic progressive EAE is necessary for studies, rather than relapsing-remitting EAE [40]. These facts point to dosing as a means of controlling the degree of EAE, which may also be true with the synthetic adjuvant. Nonetheless, the current data are sufficient to demonstrate the mycobacterial component of CFA can be replaced with mycobacterial MAMPs to induce EAE. Other experimental uses of CFA include the collagen-induced arthritis (CIA) model and for producing specific antibodies. CIA generally takes longer and has a greater role for humoral immunity than EAE which is T-cell driven, (our interest was in CMI for this study) [41]. Wherever mycobacterial adjuvancy is useful, we suspect a synthetic adjuvant could be beneficial. Indeed, intravesical injection of BCG is used to treat bladder cancer (i.e. BCG can provide MAMP-driven protection, not simply antigen-specific protection). Furthermore, BCG administration to millions of babies each year can protect not just against childhood tuberculosis, but non-specifically against other diseases [42].

Our work demonstrates that mycobacterial NOD2 and Mincle ligands contribute to the adjuvant effect of the mycobacterial cell, and that a necessarily synergistic combination of synthetic MAMPs, *N*-glycolyl MDP and GlcC14C18 can at least partly recapitulate the adjuvant effect of the whole mycobacterial cell. In addition to demonstrating the first entirely synthetic multi-MAMP mycobacterial adjuvant, we have outlined an approach to investigate the contribution of other MAMPs to adjuvant design. Moreover, the synthetic approach may be useful to probe mycobacterial immunity and immunopathogenesis.

Methods

Mice

C57BL/6 ('wild-type') as well as *Nod2*-/- mice were obtained from Jackson laboratories and were bred or used immediately for experiments. *Mincle*-/- mice breeders were provided courtesy of the laboratory of Christine Wells [25]. Mice were genotyped to confirm absence of the *Dock2* mutation recently reported in *Nod2*-/- mice [43]. All experiments used mice from 6 to 20 weeks of age. All protocols involving mice followed the guidelines of the Canadian Council on Animal Care (CCAC) and were approved by the ethics committees of the RI-MUHC.

Preparation of adjuvants and ovalbumin immunization

Complete and incomplete Freund's adjuvant were purchased from Sigma or Invivogen. In some cases, IFA was made by the experimenter from purified mineral oil and mannide monooleate (Sigma). Adjuvants were prepared on the day of immunization by emulsifying CFA (1 mg/ml *M. tuberculosis*) or IFA with a PBS solution containing 1 mg/ml ovalbumin (Endofit brand, invivogen) in a 1:1 ratio. Emulsification was accomplished using all-plastic syringes and repeated passage through an 18-G blunt-end needle. Where IFA was complemented with mycobacterial components: MDP (Invivogen) was diluted in the PBS fraction of the adjuvant before emulsification; TDM (Sigma) or GlcC14C18 [23] were dissolved in the IFA fraction before emulsification as described previously [17]; heat-killed mycobacteria in saline were diluted in PBS and added to the PBS fraction of the adjuvant before emulsification for mice to receive an equivalent of 10^8 CFU. To make heat-killed mycobacteria, cultures were grown to equivalent 600-nm absorbance at mid-log phase, were pelleted and washed three times with saline, then heat-killed at 100°C for 30 minutes and frozen at -80°C until use. Mice were injected subcutaneously with 100 µl adjuvant-antigen emulsions in the tail 1-2 cm from the body, towards the body, for sufficient and consistent drainage to the inguinal lymph nodes. Seven days after injection mice were euthanized and organs were harvested for analysis.

ELISpot and flow cytometry of lymph node cells

Lymph nodes extracted from immunized mice were gently crushed over 70-µm cell strainers to release the cells therein. Cell concentrations were determined by counting with a haemocytometer or with a BD Accuri flow cytometer. Lymph node cells (LNCs) were washed in culture medium, counted and cultured in 100 µl RPMI + 10%FBS (R10) at 250,000 or 500,000 cells per well in IFNγ ELISpot plates (R&D Systems) with or without 100 µg OVA for ~40 hours at 37°C 5% CO_2 before developing the ELISpot plates. For flow cytometry analysis, washed LNCs were cultured at 6 million cells per ml in 200 µl R10 with or without 200 µg OVA for ~40 hours at 37°C 5% CO_2, Brefeldin A (GolgiPlug™, BD) was added for an additional 5 hours, and then cells were stained and fixed (BD fixation/permeabilization buffer) for flow cytometry on ice. Intracellular staining was performed on the same or the next day using BD permeabilization buffer. See Table 1 for antibodies used for flow cytometry. A BD Fortessa X20 was used for cellular phenotyping.

Relapsing-remitting experimental autoimmune encephalomyelitis (RR-EAE)

Adjuvants were prepared similarly as above, but with myelin oligodendrocyte glycoprotein (MOG) used as antigen. Briefly, PBS solution containing 1 mg/ml MOG +/- 600 µg/ml *N*-glycolyl MDP was emulsified with CFA (1 mg/ml *M. tuberculosis*) / IFA plus 200 µg/ml

GlcC14C18 (or 20 μg/ml TDM) by back-and-forth extrusion through an 18 G two-way needle with two all-plastic syringes. 8-12 week old female C57BL/6 mice (Charles River) were induced for RR-EAE by a standard protocol: briefly, on day 0, pertussis toxin (PT) (200 ng) was administered i.v. in the tail vein, and mice were immunized with 50 μg MOG by bilateral s.c. injection in the back towards the tail with 100 μl total of an emulsification of CFA or IFA plus mycobacterial MAMPs. On day 2, mice received a second equivalent dose of PT i.v.. After about one week, EAE was scored blinded (i.e. the scorer did not know the adjuvant received by the mouse) every day according to these cumulative criteria: 0, no paralysis (normal); 0.5, partial tail weakness observed as < 50% of tail dragging when mouse walks; 1, tail paralysis observed as >50% of tail dragging as mouse walks; 2, slow righting reflex (delay < 5 seconds) when mouse is flipped; 3, very slow or absent righting reflex (> 5 seconds) or inability to bear weight with back legs observed as dragging hindquarters when walking; 3.5, partial paralysis of one or both hind limbs; 4, complete paralysis of one or both hindlimbs; 4.5, complete paralysis of one or both hind limbs plus trunk weakness; 5, weakness or paralysis of forelimbs; 6, found dead. Mice were weighed every other day during scoring. Mice reaching a score of 5 were euthanized within 24 hours. Blinding was accomplished by having one person inject the mice and another person score/weigh the mice, unaware of experimental group.

Histopathology

At the end of EAE scoring, the experiment was un-blinded and three mice from each group with matching scores were selected. These six mice were anesthetized with peritoneal ketamine injection, were perfused with PBS and formalin, and then spinal cords were extracted, equilibrated in sucrose and then frozen in OTC compound (VWR). Frozen tissue was sectioned 14-nm thick onto slides and then stained (Nissl or Luxol fast blue). Sections of good quality (20 per mouse, 5 cervical, 5 upper thoracic, 5 lower thoracic and 5 lumbar) were randomly selected and photographed with a Nikon Eclipse microscope. Randomized (blinded) Nissl stain photographs were used to quantify the area of disease in the spinal cord by subtracting the total 2D area of each tissue section with the area without cellular infiltration in white matter (thus, the difference of areas is the area with cellular infiltration). This was divided by the total area to determine the fraction or percent of diseased area.

Software, data analysis and statistics

Flow cytometry data was acquired using FACSDiva™ software (BD). FCS files were analyzed using FlowJo V10 (BD). Digital microscopy images were analyzed with ImageJ (NIH). Graphs were generated with, and routine statistical testing was accomplished with GraphPad Prism v7 or v8 (GraphPad Software Inc.). Assessment for normal data, then parametric or non-parametric analyses were applied, as indicated. Sample-size and power calculations were performed manually using Microsoft Excel. Manuscript figures were assembled with Microsoft PowerPoint.

References

1. Chase MW, Landsteiner K. Experiments on Transfer of Cutaneous Sensitivity to Simple Compounds. *Proc Soc Exp Biol Med* **49**, 688-690 (1942).

2. Chase MW. The Cellular Transfer of Cutaneous Hypersensitivity to Tuberculin. *Proc Soc Exp Biol Med* **59**, 134-135 (1945).

3. Baxter AG. The origin and application of experimental autoimmune encephalomyelitis. *Nat Rev Immunol* **7**, 904-912 (2007).

4. Constantinescu CS, Farooqi N, O'Brien K, Gran B. Experimental autoimmune encephalomyelitis (EAE) as a model for multiple sclerosis (MS). *Br J Pharmacol* **164**, 1079-1106 (2011).

5. Vogel FR. Improving Vaccine Performance with Adjuvants. *Clin Infect Dis* **30**, S266–270 (2000).

6. Adam A, Ellouz F, Ciorbaru R, Petit JF, Lederer E. Peptidoglycan adjuvants: minimal structure required for activity. *Z Immunitatsforsch Exp Klin Immunol* **149**, 341-348 (1975).

7. Coulombe F, *et al.* Increased NOD2-mediated recognition of *N*-glycolyl muramyl dipeptide. *J Exp Med* **206**, 1709-1716 (2009).

8. Raymond JB, Mahapatra S, Crick DC, Pavelka MS, Jr. Identification of the namH gene, encoding the hydroxylase responsible for the N-glycolylation of the mycobacterial peptidoglycan. *J Biol Chem* **280**, 326-333 (2005).

9. Mahapatra S, Crick DC, McNeil MR, Brennan PJ. Unique structural features of the peptidoglycan of Mycobacterium leprae. *J Bacteriol* **190**, 655-661 (2008).

10. Essers L, Schoop HJ. Evidence for the incorporation of molecular oxygen, a pathway in biosynthesis of *N*-glycolylmuramic acid in *Mycobacterium phlei*. *Biochim Biophys Acta* **544**, 180-184 (1978).

11. Hansen JM, *et al. N*-glycolylated peptidoglycan contributes to the immunogenicity but not pathogenicity of Mycobacterium tuberculosis. *J Infect Dis* **209**, 1045-1054 (2014).

12. Girardin SE, *et al.* Nod2 is a general sensor of peptidoglycan through muramyl dipeptide (MDP) detection. *J Biol Chem* **278**, 8869-8872 (2003).

13. Miceli-Richard C, *et al.* CARD15 mutations in Blau syndrome. *Nat Genet* **29**, 19-20 (2001).

14. Ogura Y, *et al.* A frameshiftmutation in NOD2 associated with susceptibility to Crohn's disease. *Nat Lett* **411**, 603-606 (2001).

15. Austin CM, Ma X, Graviss EA. Common nonsynonymous polymorphisms in the NOD2 gene are associated with resistance or susceptibility to tuberculosis disease in African Americans. *J Infect Dis* **197**, 1713-1716 (2008).

16. Zhang FR, *et al.* Genomewide association study of leprosy. *N Engl J Med* **361**, 2609-2618 (2009).

17. Shenderov K, *et al.* Cord factor and peptidoglycan recapitulate the Th17-promoting adjuvant activity of mycobacteria through Mincle/CARD9 signaling and the inflammasome. *J Immunol* **190**, 5722-5730 (2013).

18. Ishikawa E, *et al.* Direct recognition of the mycobacterial glycolipid, trehalose dimycolate, by C-type lectin Mincle. *J Exp Med* **206**, 2879-2888 (2009).

19. Miyake Y, *et al.* C-type lectin MCL is an FcRgamma-coupled receptor that mediates the adjuvanticity of mycobacterial cord factor. *Immunity* **38**, 1050-1062 (2013).

20. Bekierkunst A. Acute Granulomatous Response Produced in Mice by Trehalose-6,6-Dimycolate. *J Bacteriol* **96**, 958-961 (1968).

21. Shigeru K, Tsunehiko F, Hidefumi Y, Masahiko F, Ichiro A, Yuichi Y. Synthesis of Muramyl Dipeptide Analogs with Enhanced Adjuvant Activity. *Bull Chem Soc Japan* **53**, 2570-2577 (1980).

22. Xing S, Gleason JL. A robust synthesis of N-glycolyl muramyl dipeptide via azidonitration/reduction. *Org Biomol Chem* **13**, 1515-1520 (2015).

23. Decout A, *et al.* Rational design of adjuvants targeting the C-type lectin Mincle. *Proc Natl Acad Sci U S A* **114**, 2675-2680 (2017).

24. Divangahi M, *et al.* NOD2-Deficient Mice Have Impaired Resistance to Mycobacterium tuberculosis Infection through Defective Innate and Adaptive Immunity. *J Immunol* **181**, 7157-7165 (2008).

25. Wells CA, *et al.* The Macrophage-Inducible C-Type Lectin, Mincle, Is an Essential Component of the Innate Immune Response to Candida albicans. *The Journal of Immunology* **180**, 7404-7413 (2008).

26. Janeway CA. Approaching the Asymptote? Evolution and Revolution in Immunology. *Cold Spring Harb Symp Quant Biol* **54**, 1-13 (1989).

27. Odendall C, Kagan JC. Host-Encoded Sensors of Bacteria: Our Windows into the Microbial World. *MicrobiolSpectrum* **7**, (2019).

28. Yonekawa A, *et al.* Dectin-2 Is a Direct Receptor for Mannose-Capped Lipoarabinomannan of Mycobacteria. *Immunity* **41**, 402–413 (2014).

29. Decout A, *et al.* Deciphering the molecular basis of mycobacteria and lipoglycan recognition by the C-type lectin Dectin-2. *Sci Rep* **8**, 16840 (2018).

30. Stamm CE, Collins AC, Shiloh MU. Sensing of Mycobacterium tuberculosis and consequences to both host and bacillus. *Immunol Rev* **264**, 204-219 (2015).

31. Prinz M, *et al.* Innate immunity mediated by TLR9 modulates pathogenicity in an animal model of multiple sclerosis. *J Clin Invest* **116**, 456-464 (2006).

32. Reynolds JM, *et al.* Toll-like receptor 2 signaling in CD4(+) T lymphocytes promotes T helper 17 responses and regulates the pathogenesis of autoimmune disease. *Immunity* **32**, 692-702 (2010).

33. Miranda-Hernandez S, *et al.* Role for MyD88, TLR2 and TLR9 but not TLR1, TLR4 or TLR6 in experimental autoimmune encephalomyelitis. *J Immunol* **187**, 791-804 (2011).

34. Shaw PJ, *et al.* Signaling via the RIP2 adaptor protein in central nervous system-infiltrating dendritic cells promotes inflammation and autoimmunity. *Immunity* **34**, 75-84 (2011).

35. Collins Angela C, *et al.* Cyclic GMP-AMP Synthase Is an Innate Immune DNA Sensor for Mycobacterium tuberculosis. *Cell Host & Microbe* **17**, 820-828 (2015).

36. Watson Robert O, *et al.* The Cytosolic Sensor cGAS Detects Mycobacterium tuberculosis DNA to Induce Type I Interferons and Activate Autophagy. *Cell Host & Microbe* **17**, 811-819 (2015).

37. Bafica A, Scanga CA, Feng CG, Leifer C, Cheever A, Sher A. TLR9 regulates Th1 responses and cooperates with TLR2 in mediating optimal resistance to Mycobacterium tuberculosis. *J Exp Med* **202**, 1715-1724 (2005).

38. Chen Z, Wang W, Liang J, Wang J, Feng S, Zhang G. Association between toll-like receptors 9 (TLR9) gene polymorphism and risk of pulmonary tuberculosis: meta-analysis. *BMC Pulm Med* **15**, 57 (2015).

39. Eisenbarth SC, Piggott DA, Huleatt JW, Visintin I, Herrick CA, Bottomly K. Lipopolysaccharide-enhanced, toll-like receptor 4-dependent T helper cell type 2 responses to inhaled antigen. *J Exp Med* **196**, 1645-1651 (2002).

40. Berard JL, Wolak K, Fournier S, David S. Characterization of relapsing-remitting and chronic forms of experimental autoimmune encephalomyelitis in C57BL/6 mice. *Glia* **58**, 434-445 (2010).

41. Brand DD, Latham KA, Rosloniec EF. Collagen-induced arthritis. *Nat Protoc* **2**, 1269-1275 (2007).

42. Kleinnijenhuis J, *et al.* Bacille Calmette-Guerin induces NOD2-dependent nonspecific protection from reinfection via epigenetic reprogramming of monocytes. *Proc Natl Acad Sci U S A* **109**, 17537-17542 (2012).

43. Wong SY, *et al.* B Cell Defects Observed in Nod2 Knockout Mice Are a Consequence of a Dock2 Mutation Frequently Found in Inbred Strains. *J Immunol* **201**, 1442-1451 (2018).

Acknowledgments

We would like to thank the Containment Level 3 platform of the Research Institute of the McGill University Health Centre (RI-MUHC) for providing the needed facilities and intellectual support. Similarly, we thank the Immunophenotyping platform of the RI-MUHC for cytometers and advice. We are very grateful to Christine Wells (University of Melbourne, Australia) for providing *Mincle*-KO mice and to Alexiane Decout for preparing GlcC14C18. For tutelage and technical assistance, J.Y.D. is thankful to Damien Montamat-Sicotte, Ourania Tsatas, Sarah Danchuk, Iain Roe, Andréanne Lupien, Nimara Asbah, and Daniel Houle. J.Y.D. was personally supported by the Canadian Institutes of Health Research (CIHR) Canada Graduate Scholarship – Master's Program, Fonds de Recherche du Québec – Santé (FRQ-S) Doctoral Training Award, RI-MUHC studentships (Master's and Ph.D.) and scholarships from the McGill Department of Microbiology and Immunology. Research activities were funded by CIHR foundation grant held by M.B. and a CIHR grant held by S.D.

Author Contributions

Conceptualization, J.Y.D. and M.B.; Methodology, J.Y.D. and J.G.Z.; Investigation, J.Y.D., F.M. and J.G.Z.; Resources, S.D., J.N. and M.B.; Writing – Original Draft, J.Y.D. and M.B.; Writing – Review & Editing, J.Y.D., F.M., J.G.Z., S.D., J.N. and M.B.; Visualization, J.Y.D.; Supervision, S.D. and M.B.; Funding acquisition, J.Y.D., S.D. and M.B.

Competing Interests

The authors have no competing interests

Figure Legends

Figure 1. CFA-dependent cell-mediated immune responses as a function of mycobacterial *namH*. **A**, PGN of 'wild-type' H37Rv *M. tuberculosis* (left) and PGN of the Δ*namH* mutant (right). The MDP motif is drawn in red, and the site of *N*-glcolylation is in bold font. With NamH, *N*-glycolylation was shown on ~70% of muramic acid residues, with *N*-acetylation on the remaining ~30% [8, 11]. **B**, immunization scheme (relevant to figs. 1-5): C57Bl/6J mice were immunized with adjuvant emulsion containing OVA by s.c. injection at the base of the tail, and after seven days, inguinal (draining) lymph nodes were harvested. Lymph node cells were cultured *ex vivo* with or without OVA to examine OVA-specific cytokine response by flow cytometry or ELISpot. **C**, cytokine production from CD4+CD8- lymph node cells of mice immunized against OVA with heat-killed *M. tuberculosis* strain H37Rv, H37Rv Δ*namH*, or IFA alone, seven days prior. Shown are data pooled from four separate experiments, from individual mice, with averages +/- SEM. p-values were calculated with two-tailed student's t-tests. *p<0.05; **p<0.01; ns, not significant, p>0.05. For IFA + H37Rv, IFA + H37Rv Δ*namH*, and IFA alone, N = 31, 27 and 16, respectively.

Figure 2. CFA-dependent cell-mediated immune responses as a function of host *Nod2*. Cytokine production from CD4+CD8- lymph node cells of *Nod2*+/+ and *Nod2*-/- mice immunized against OVA with CFA or IFA seven days prior. Shown are data representative of two independent experiments, from individual mice with averages +/- SEM. p-values were calculated with two-tailed student's t-tests. *p<0.05; **p<0.01; ns, not significant, p>0.05. For CFA *Nod2*+/+, CFA *Nod2*-/-, IFA *Nod2*+/+ and IFA *Nod2*-/-, N = 12, 13, 9 and 7, respectively.

Figure 3. CFA-dependent cell-mediated immune responses as a function of host *Mincle*. Cytokine production from CD4+CD8- lymph node cells of *Mincle*+/+ and *Mincle*-/- mice immunized against OVA with CFA or IFA seven days prior. Shown are data pooled from two independent experiments, from individual mice, with averages +/- SEM. p-values were calculated with two-tailed student's t-tests. *p<0.05; **p<0.01; ns, not significant, p>0.05. For CFA *Mincle*+/+, CFA *Mincle*-/-, IFA *Mincle*+/+ and IFA *Mincle*-/-, N = 14, 16, 15 and 11, respectively.

Figure 4. *Mincle*-dependent inflammation from TDM is not observed with synthetic TDM analogue GlcC14C18. **A**, TDM molecular structure. **B**, GlcC14C18 molecular structure. **C,** representative tail injection site pathology seven days after injection of 10 μg TDM or 10 μg GlcC14C18 in IFA-PBS emulsion. Pictures are representative of 3 mice per group.

Figure 5. Complementation of IFA with synthetic mycobacterial MAMPs. Cytokine production from CD4+CD8- lymph node cells of wild-type mice immunized against OVA seven days prior with IFA + 30 µg *N*-glycolyl MDP (N=6), IFA + 30 µg *N*-glycolyl MDP + 10 µg GlcC14C18 (N=7), IFA + 30 µg *N*-glycolyl MDP + 30 µg GlcC14C18 (N=7), or CFA (N=7). Shown are data from individual mice, with averages +/- SEM.

Figure 6. RR-EAE induced by IFA+GlcC14C18+MDP. A, experimental timeline. **B**, average EAE score +/- SEM over time of mice induced with CFA (N=15) or IFA + 10 µg GlcC14C18 + 30 µg *N*-glycolyl MDP (N=15). Mice were euthanized on day 28 post injection. **C**, Cumulative EAE score, obtained by adding the EAE score of each mouse over each of the 28 days. Lines represent averages +/- SEM. p-value was calculated with two-tailed student's t-tests. **p = 0.0022

Figure 7. Spinal cord pathology in RR-EAE mice induced by IFA+GlcC14C18+MDP. A, Nissl and Luxol fast blue (LFB) stains of spinal cord sections from RR-EAE-induced mice at day 28 post injection, having an EAE score of 3.5 upon euthanasia. Red boxes highlight cellular infiltration and spatially associated demyelination of the white matter seen by Nissl and LFB staining, respectively. **B**, Quantitative spinal cord pathology per EAE score upon euthanasia. Statistical significance was determined by Tukey's multiple comparisons test. *p<0.05 and ****p<0.0001 (adjusted for multiple comparisons). N=40 for each group (20 from CFA and 20 from synthetic adjuvant of equivalent EAE scores). Lines indicate averages +/- SEM **C**, Quantitative spinal cord pathology per adjuvant. Statistical significance was tested with two-tailed unpaired Welch's t-test; a power calculation for given variances and N=60 per group indicated an ability to discern +/- 15% difference vs. CFA control. Lines indicate averages +/- SEM.

Tables

Table 1. Flow cytometry antibodies

Target	Brand	Clone	Fluorochrome
CD3ε	BD	145-2C11	PE
CD4	BD	GK1.5	BV786
CD8α	BD	53-6.7	BV711
CD19	Biolegend	6D5	PE-Dazzle594
B220/CD45R	BD	RA3-6B2	BUV737
IFN-γ	Biolegend	XMG1.2	APC
IL-2	BD	JES6-5H4	BV605
IL-4	eBiosciences	BVD6-24G2	PE-Cy7
IL-17A	BD	TC11-18H10	BUV395
IL-10	BD	JES5-16E3	FITC

Supplementary Information

Supplemental Method: Bone marrow-derived dendritic cells (BMDCs)

Bone marrow was extracted from mice by flushing femora and tibiae with PBS + 2% BSA + 2% glucose using a 25-G syringe. Red blood cells were lysed and remaining bone marrow cells were filtered through 70 µm cell strainer. Cells were cultured at 500,000 cells / ml R10 with 20 ng/ml murine rGM-CSF (PeproTech); cells were fed on day 3 with R10 + rGM-CSF, and on day 6 with R10 alone. On day 7, loosely adherent cells were harvested by gentle pipetting and used in assays.

Supplemental Figure Legends

Figure S1. Flow cytometry gating strategy for lymph node cells. Shown is representative gating and data from an OVA-stimulated sample.

Figure S2. CFA-dependent lymphoproliferation, IL-4 and IL-10 as a function of mycobacterial *namH*. These data are from the same set shown in fig. 1B (refer to fig. 1B legend for details). p-values were calculated with two-tailed student's t-tests.

Figure S3. Contribution of *namH* to the mycobacterial portion of OVA-specific IFN-γ elicited by CFA. These transformed data are from the same set shown in fig. 1B (refer to fig. 1B legend for details). **A**, result was obtained from %IFN-γ+ data by subtracting the average IFA background from all CFA data, and plotting the results as % of IFA+H37Rv 'wild-type'. **B**, result was obtained from # IFN-γ+ data by subtracting the average IFA background from all CFA data, and plotting the results as % of IFA+H37Rv 'wild-type'.

Figure S4. CFA-dependent ELISpot IFN-γ, lymphoproliferation, IL-4 and IL-10 as a function of host *Nod2*. **A**, IFN-γ ELISpot of total lymph node cells of immunized mice produced in an independent experiment. p-values were calculated with two-tailed student's t-tests. *p<0.05 and ***p<0.0005. For CFA *Nod2*+/+, CFA *Nod2*-/-, IFA *Nod2*+/+ and IFA *Nod2*-/-, N = 6, 8, 6 and 6, respectively. **B-C**, data are from the same set shown in fig. 2 (refer to fig. 2 legend for details).

Figure S5. CFA-dependent lymphoproliferation, IL-4 and IL-10 as a function of host *Mincle*. These data are from the same set shown in fig. 3 (refer to fig. 3 legend for details).

Figure S6. TDM-induced injection site pathology. Tail injection site pathology seven days after injection of 1 µg TDM or 10 µg TDM in IFA-PBS emulsion, or CFA control. Pictures are representative of 5 mice per group.

Figure S7. Semi-quantification of *Mincle*-dependent inflammation from TDM. These data are from the same set shown in fig. 4C (refer to fig. 4C legend for more details). **A**, injection site pathology over time (scores were given by these criteria: 0, normal; 1, any mark/discoloration at site; 2, obvious swelling; 3, 2+abnormal skin). **B**, scores from A for each day added together. Shown are means +/- SD. N=3 for all groups.

748 **Figure S8. Murine BMDCs respond to *N*-glycolyl MDP, TDM and GlcC14C18**
749 **synergistically.** 200,000 BMDCs were transferred per well into 96-well plates precoated with
750 50 ng/well of TDM or GlcC14C18 by dissolving in isopropanol and drying (lipid-free conditions
751 used wells treated with isopropanol alone). Where present, MDP is 1 µg/ml. BMDCs were
752 incubated with stimulants for 6 hours at 37°C, 5% CO_2 before supernatant was removed for
753 ELISA analysis. Shown are averages +/- SEM of 3-6 individually stimulated and assayed wells.
754
755 **Figure S9. Adjuvant-dependent lymphoproliferation and ELISpot IFN-γ.** These data are
756 from the same set shown in fig. 5 (refer to fig. 5 legend for details).
757
758 **Figure S10. Complementation of IFA with fixed GlcC14C18 dose, increasing *N*-glycolyl**
759 **MDP dose. A**, lymphoproliferation and **B**, cytokine production from CD4+ lymph node cells of
760 wild-type mice immunized against OVA seven days prior with IFA (N=4), IFA + 10 µg
761 GlcC14C18 (N=7), IFA + 10 µg GlcC14C18 + 1 µg MDP (N=6), or IFA + 10 µg GlcC14C18 +
762 3 µg MDP (N=7). Shown are data from individual mice, with averages +/- SEM.
763
764 **Figure S11. Descriptive statistics for RR-EAE induced by IFA+GlcC14C18+MDP.** These
765 data are from the same set shown in fig. 6 (refer to fig. 6 legend for details). **A**, average weight
766 +/- SEM over time of mice. **B**, maximum EAE score reached on any day by mice, as of day 28.
767 **C**, disease course of mice selected for spinal cord histopathology.
768
769 **Figure S12. Descriptive statistics for RR-EAE induced by IFA+TDM+MDP. A**, average
770 EAE score +/- SEM over time of mice induced with CFA (N=13) or IFA + 1 µg TDM + 30 µg
771 *N*-glycolyl MDP (N=13). Mice were euthanized on day 27 post injection. **B**, cumulative EAE
772 score, obtained by adding the EAE score of each mouse over each of the 27 days. Lines
773 represent averages +/- SEM. **C**, average weight +/- SEM over time of mice. **D**, maximum EAE
774 score reached on any day by mice, as of day 27.

FIG. 1

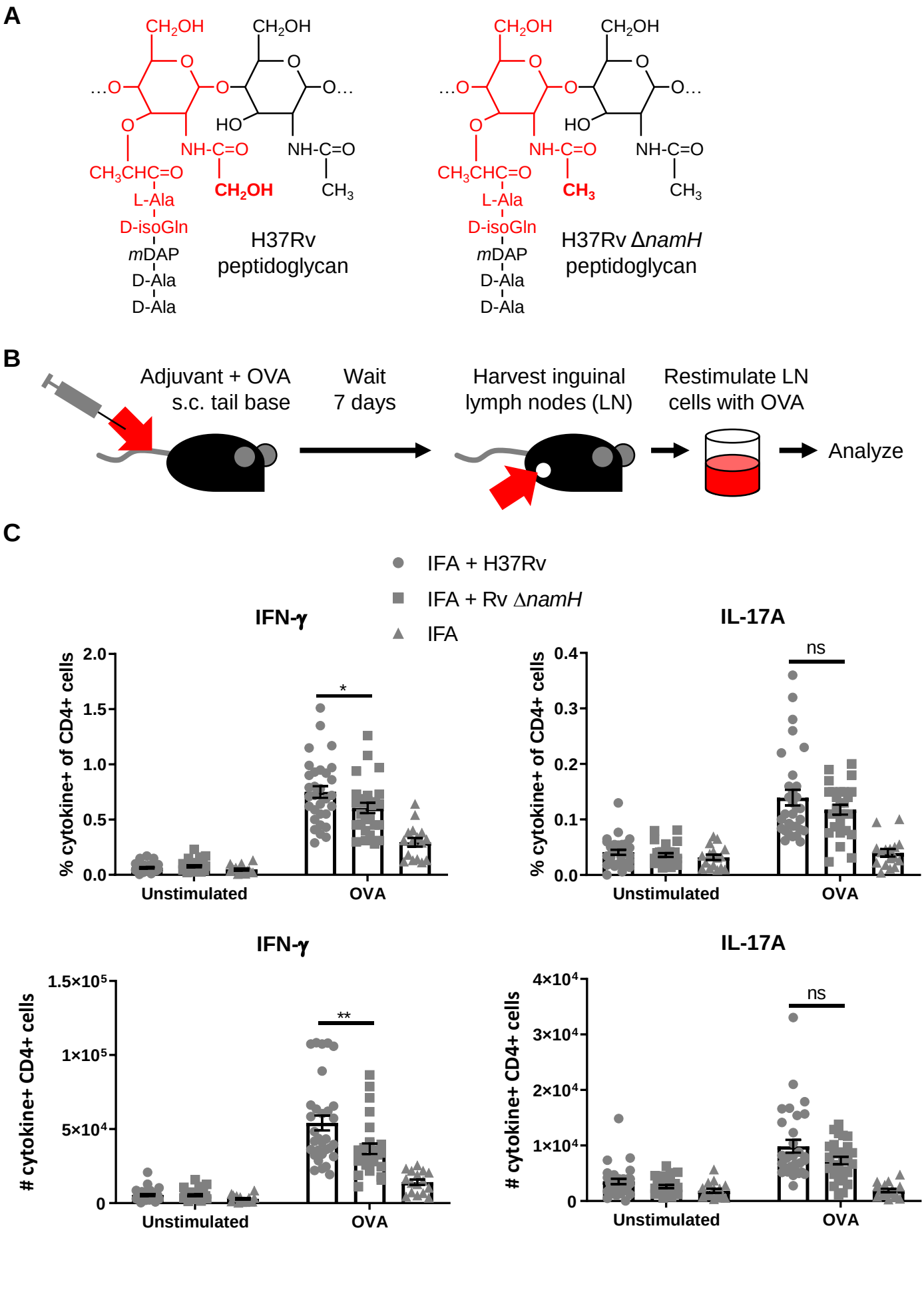

FIG. 2

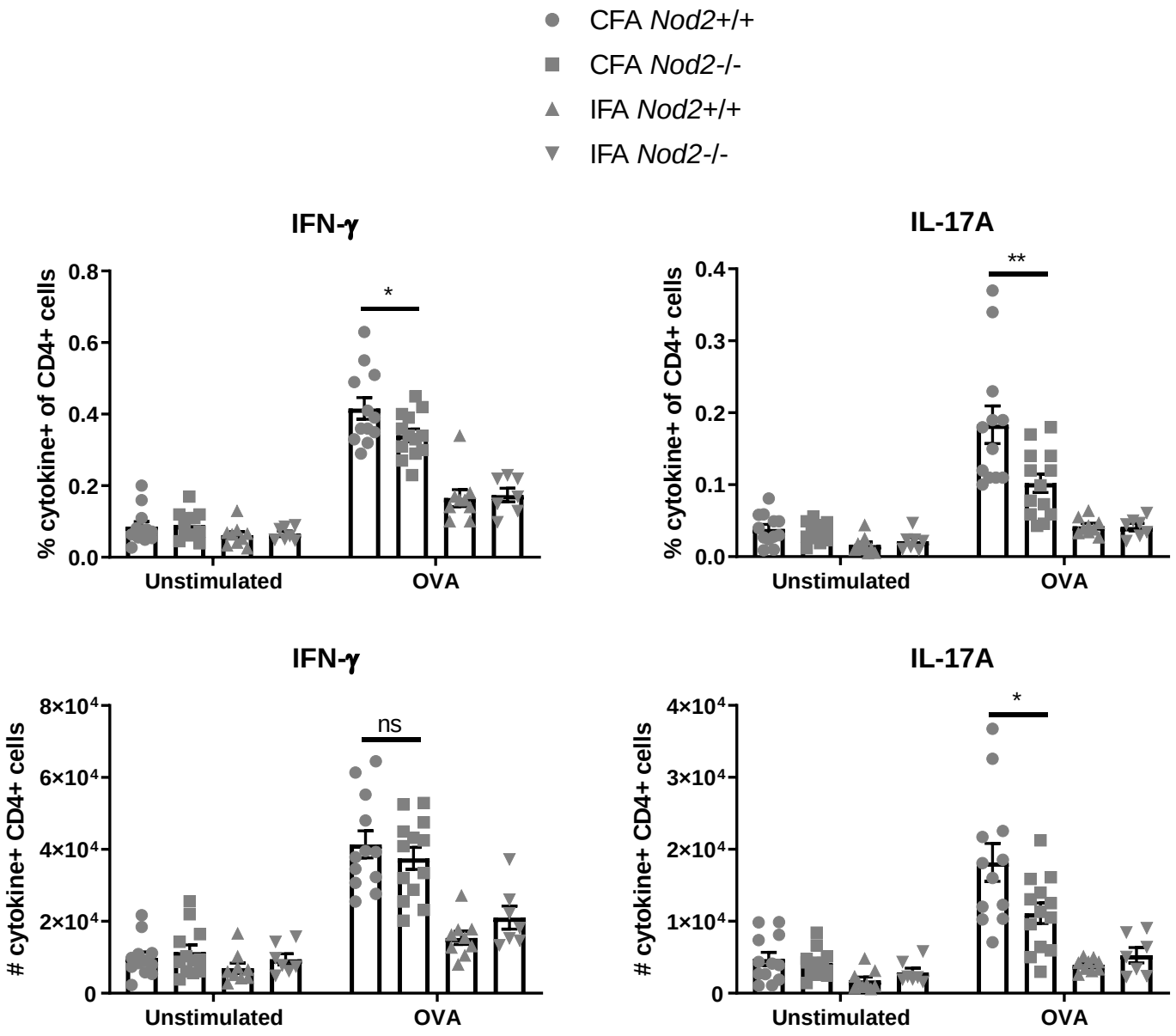

FIG. 3

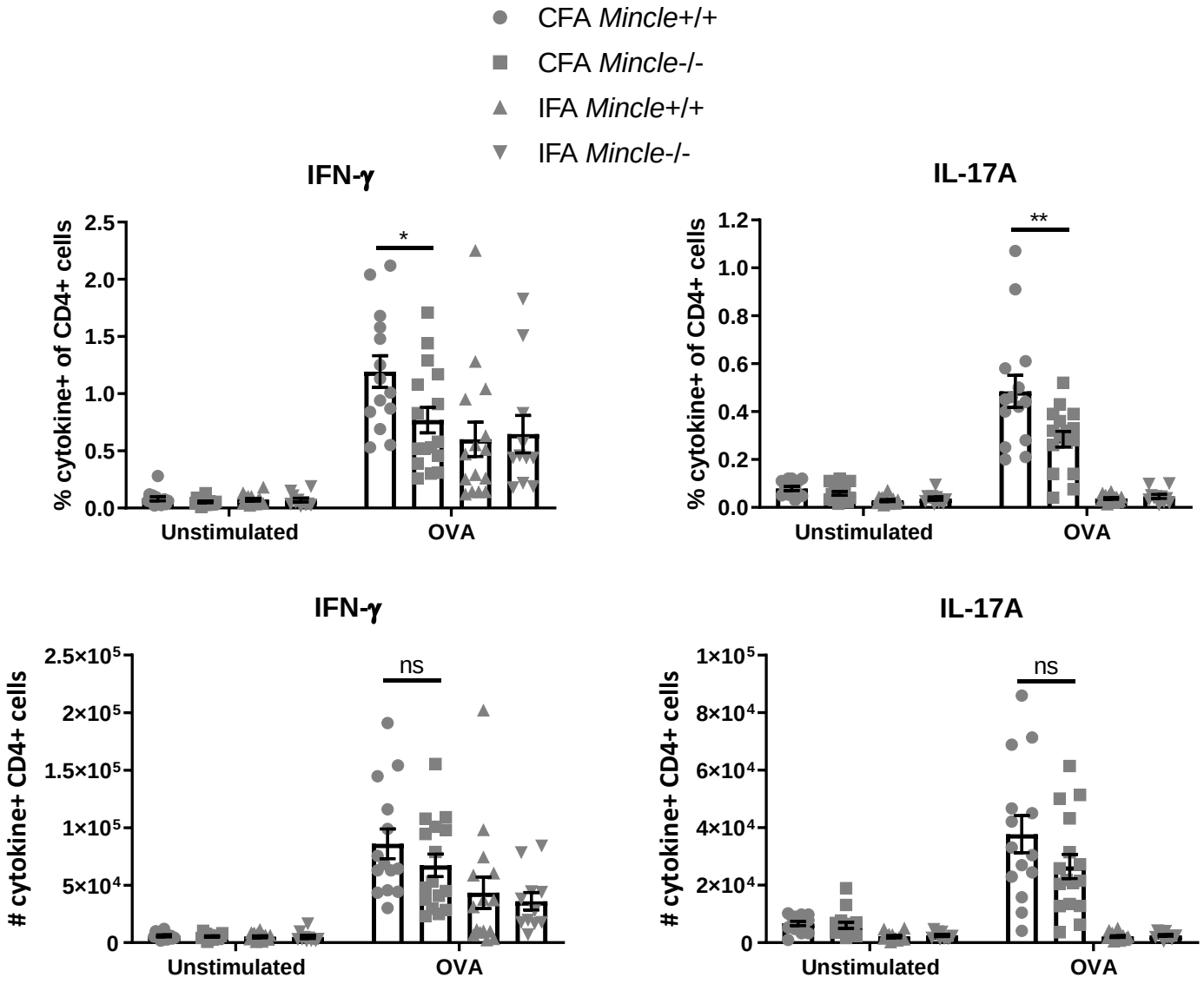

FIG. 4

A

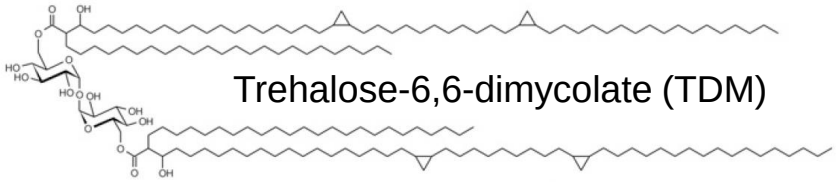

B

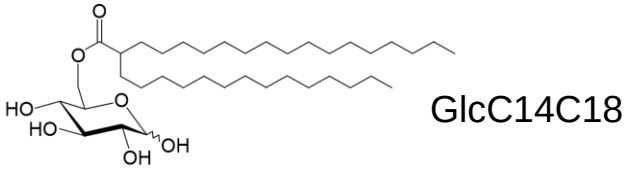

C

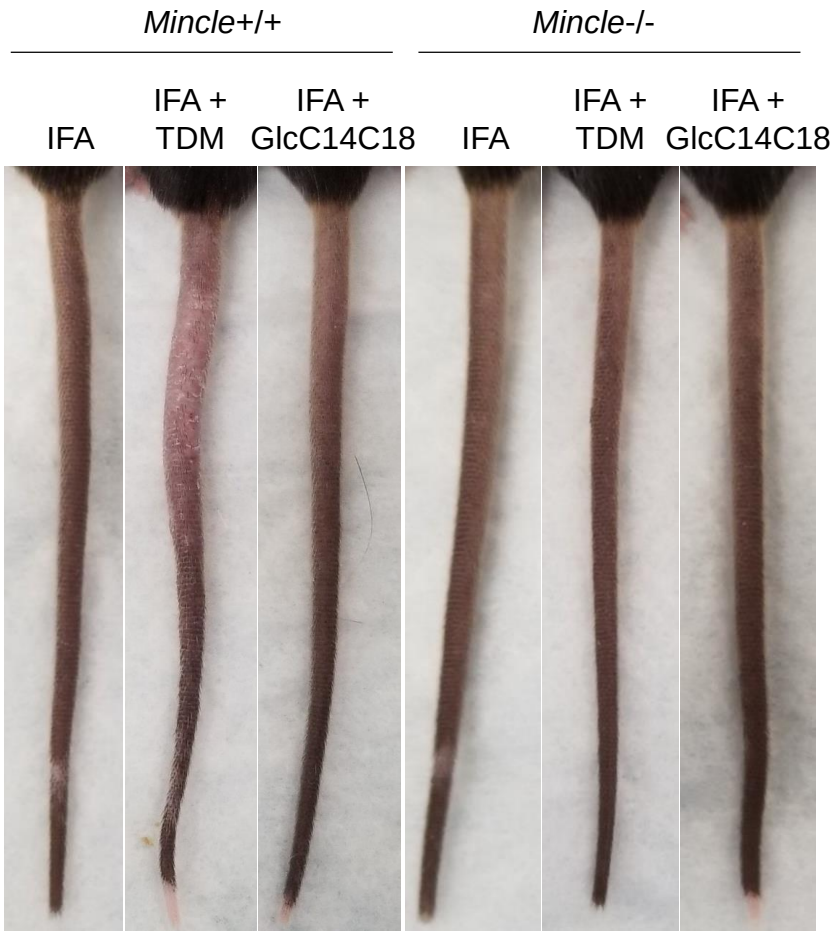

FIG. 5

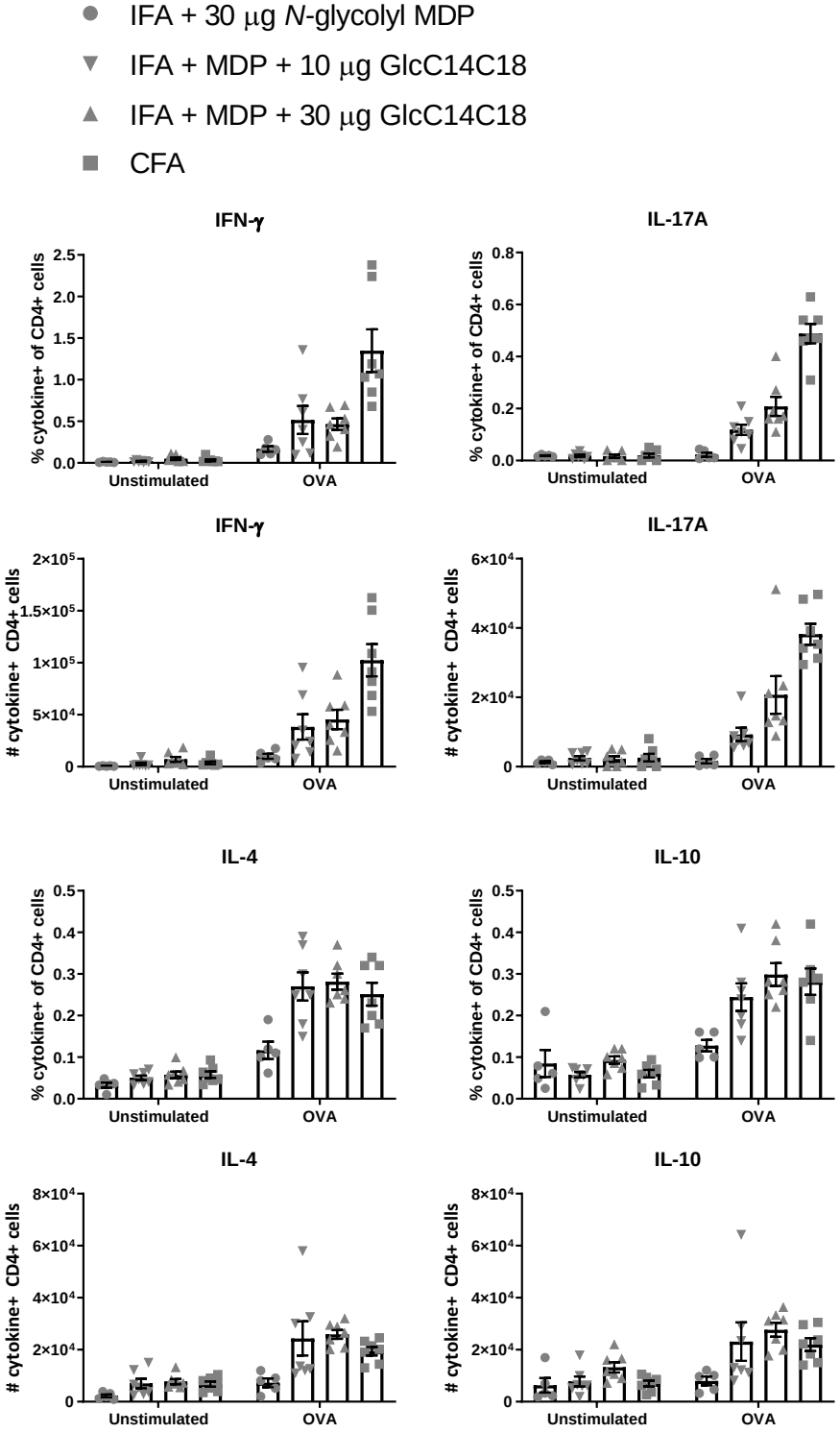

FIG. 6

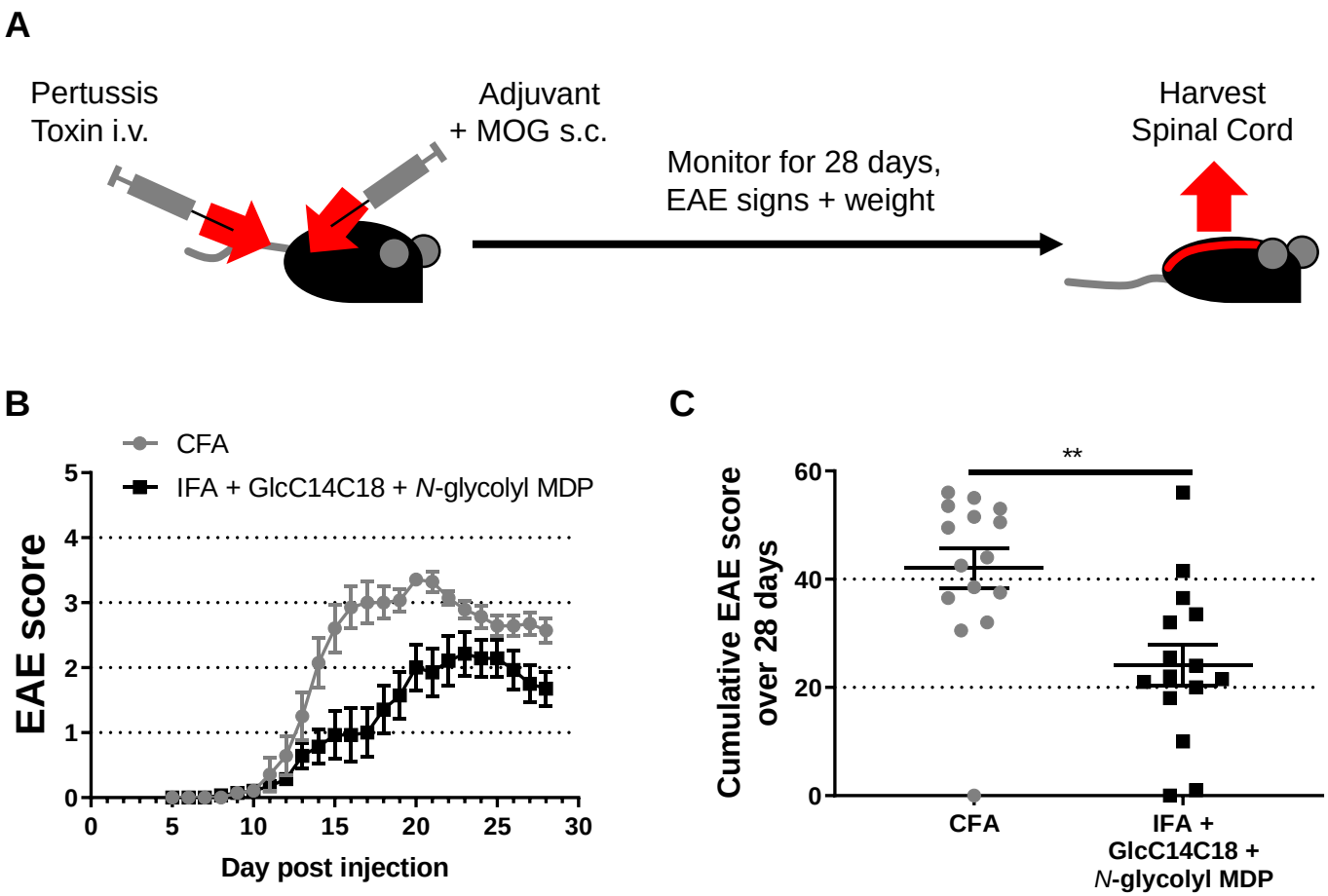

FIG. 7